



# Troubleshooting Noise and Vibration Issues of a Metro Braking System

Gianluca Megna<sup>1</sup> · Andrea Bracciali<sup>1</sup>

Received: 29 December 2022 / Revised: 2 March 2023 / Accepted: 13 March 2023  
© The Author(s) 2023

## Abstract

**Purpose** The braking system used on a recently upgraded metro vehicle showed very high low-frequency noise and vibrations levels in service affecting passengers' comfort and leading to both brake calliper lever failures and to premature wear of brake pads. The characteristics of the phenomenon were such that it was classified as a *groan noise* type. As brake pads with different characteristics were tested trying to attenuate the issue without success, the paper describes the approach adopted by the authors to tackle the issue.

**Methods** The dynamic behaviour of all the components involved during the braking phase (wheelset, callipers, brake discs and part of the bogie frame) was analysed by numerical simulations and tests during service, finding a coincidence of the natural frequencies of the wheelset and the brake support. As this resonance was believed to be the root cause of the problem, a number of structural modifications were proposed.

**Results and Conclusions** After a careful selection process that included robustness and sensitivity analyses, the accepted modification proved to be effective in solving the issue and was applied with satisfaction to the whole fleet.

**Keywords** Railway · Metro · Braking · Groan noise · Vibration · Modal analysis · Operational deflection shapes · Structural modification · Sensitivity analysis · Robustness

## Foreword

## Introduction

Due to the tendency of increasing vehicle speed, research about railway vehicle noise is today mainly focused on the analysis of aerodynamic noise [1, 2]. However, noise generated during the braking phases can be very annoying for passengers within the vehicles and on station platforms, especially for underground systems [3] due to sound reflections generated in tunnels that increase sound pressure for a given sound power. The issue may become relevant for human health in case of long-time exposures (e.g. drivers) especially if high-pitch tonal phenomena such as squeal noise are generated.

Measurements performed during braking of a high-speed train have shown sound pressure levels above 100 dB in a large range of frequencies [4, 5] due to squeal noise. The

authors also have found important differences between three different kinds of pads, showing how the characteristics of the friction material play a major role in the generation of squeal noise.

The frictional behaviour of the pair brake pad/brake disc is a complex matter due to the variability over the time of the involved parameters, i.e. contact pressure, contact area, temperature and the friction coefficient [6]. Finite element method and complex modal analysis are used to investigate the issue and predict the unstable vibrational modes [7–11].

Apart from squeal noise, other kinds of instability behaviour can be generated during the braking phase. Low-frequency vibrations are responsible for the so-called groan noise, which is not very common in railway brakes, while several theoretical and experimental studies can be found for automotive vehicles [12–15].

The present paper deals with a case of loud groan noise found during the braking phases of a railway vehicle. It occurred when a large upgrade project was applied to a metro vehicle built in the 1970s to extend its useful life and one of the major changes was a completely new trailer bogie that included wheelsets with two brake discs fitted on the axle.

✉ Gianluca Megna  
gianluca.megna@unifi.it

<sup>1</sup> Department of Industrial Engineering, Università degli Studi di Firenze, Florence, Italy

Soon after the beginning of the service, a loud low-frequency tonal noise appeared during service braking, together with high vibration levels generating failures on the calliper and fast brake pads crumbling.

The analysis of the mechanical system and noise characteristics led to the conclusion that the phenomenon falls in the groan noise category. A specifically designed test campaign confirmed high acceleration levels, while measurements performed with electrical resistance strain gauges showed very high stress levels in the brake units.

As an immediate structural mitigation measure, the authors proposed a reinforcing modification to brake calliper components. This short-term provision proved to be successful as further failures were prevented, leaving nevertheless unaffected the cause of noise and vibration (N and V) issues that continued to be present.

The paper is the extended version of the conference paper [16] and describes the approach used to eliminate the N and V issue, including findings, modelling and tuning of the proposed solutions. A comprehensive sensitivity analysis allowed to define the robustness of the different solutions and to identify the most promising one. The accepted modification was then implemented throughout the entire fleet with complete satisfaction.

## Braking N and V Classification

Friction braking may introduce unpleasant side effects such as degraded dynamics, thermal effects and wear of the involved components. Higher noise and vibrations may originate at the sliding contact between the friction component, i.e. the brake pad, and the rotating part, the disc brake or the wheel in the case of brake blocks.

Both groan noise and squeal noise are generated by unstable (self-excited) vibrations, caused by the nonlinear behaviour of the brake pad/brake disc pair. Specifically, the *stick-slip* phenomena, led by the negative slope of the friction force vs. sliding speed curve above the adhesion limit, the *sprag-slip* phenomena occurring even if the coefficient of friction is independent from the relative speed and *flutter* due to the interaction of vibrating modes can be the mechanisms of generation of unstable vibrations [17, 18].

The mechanism responsible for the squeal and the groan noise is not the same. As consequence they appear at different frequencies and with different consequences:

- The squeal noise occurs at high frequencies ( $> 1$  kHz), mainly due to complex flutter mechanisms involving out-of-plane (bending) elastic displacements of the brake disc, which vibrates at its eigenfrequencies generating a high pitch and very loud and tonal noise. Squeal noise is very annoying, but has limited consequences on struc-

tural components as the amplitude of vibrations does not generate noticeable stresses;

- The groan noise occurs at lower frequencies ( $< 1$  kHz), and it is correlated to an in-plane motion of the brake disc and the stick-slip phenomena is considered responsible for the excitation. The disc can be considered rigid and all the flexibility of the system can be attributed to the calliper components. High-intensity vibrations are generated which are transmitted by the structure and cause a loss of comfort for the passenger inside the vehicles [19].

Groan noise occurs at low speed and could be affected by both the friction properties of the materials involved and the mechanical properties of braking equipment [20, 21], especially the stiffness of the components supporting the brake callipers and the characteristics of the suspensions. Therefore, groan noise can be tackled by acting on the dynamic response of the whole system instead of limiting the analysis to the friction behaviour of the contact surfaces between brake discs and brake pads [22, 23].

In the present case, all the attempts to solve the issue, mainly present at the one-third octave band centred at 250 Hz, by changing the friction material, i.e. the brake pads, were not effective, showing a possible correlation between the vibrations and the global dynamic behaviour of all the following components (Fig. 1):

- The *wheelset*, including axle, wheels and brake discs, that cannot be considered rigid.
- The *bogie frame* (or its sub-parts) and the connecting interfaces with the braking equipment.
- The *brake support*, a cast steel component bolted to the bogie frame which makes the bogie frame adaptable to different brake units.
- The *brake unit*, suspended with links to the brake support.

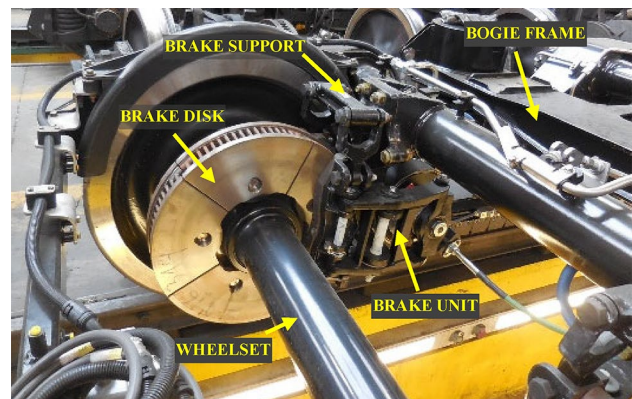


**Fig. 1** General view of the trailer bogie with indication of the main components



Fig. 2 Brake unit installed on the brake test bench

## Wheelset and Braking System Dynamic Analysis

### Behaviour of the Braking System on the Test Rig

The brake unit discussed in this paper is used since many years in many different projects without any problem, and this research deals with the very first occurrence of high noise generated by the vehicle equipped with this component. During qualification phases the brake unit was obviously tested but no noise issues were observed during the type tests on the supplier test bench (Fig. 2). This can be explained by observing that the bench did not fully reproduce the actual configuration of the bogie as (i) the wheelset was absent, (ii) the brake disc was installed on a shaft which does not reproduce dynamically its real boundary conditions, (iii) the brake unit was connected to the bench with a different brake support (welded instead of casted) and *iv*) the bogie frame was replaced by the much stiffer bench structure.

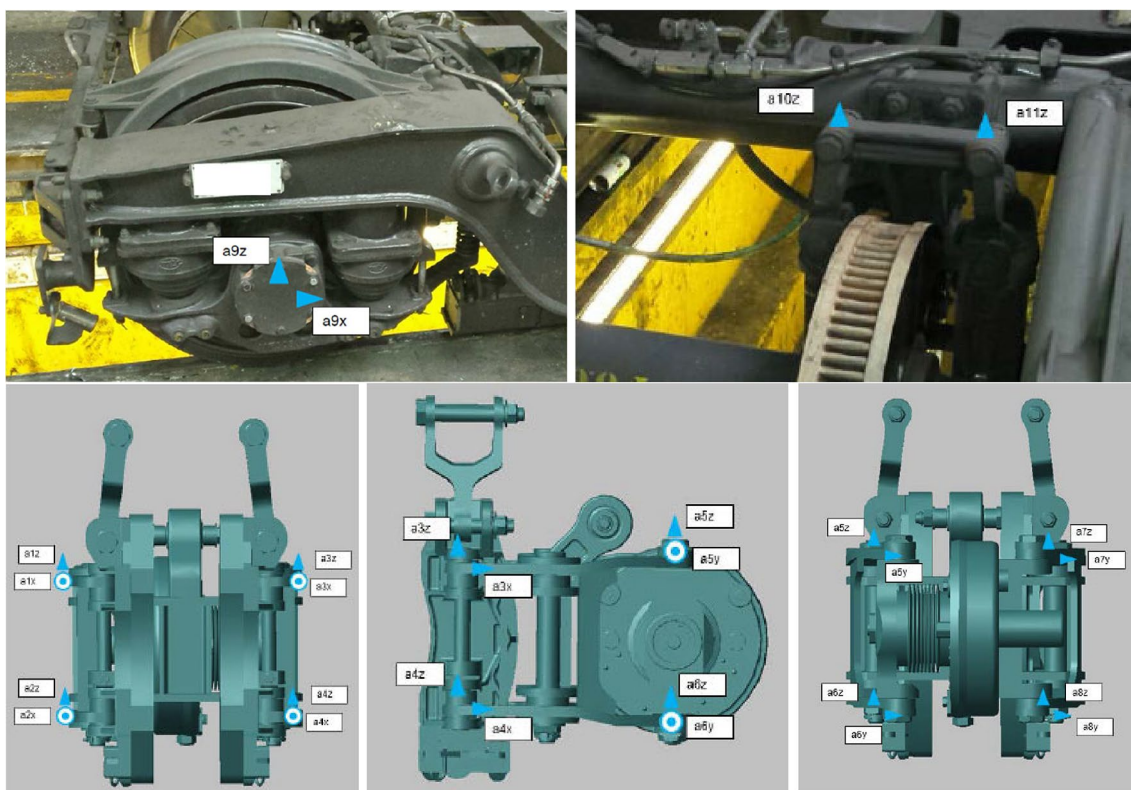
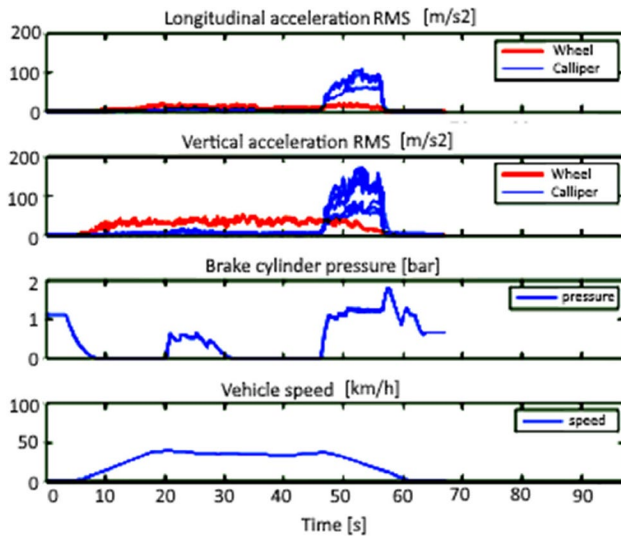


Fig. 3 Arrangement of sensor for line tests. Top left: accelerometer position on the wheelset. Top right: view of the braking unit with indication of the accelerometers position on the brake support. Bottom: accelerometers position on the brake unit





**Fig. 4** Signals recorded during test runs. From top to bottom: longitudinal RMS vibrations on wheel and calliper, vertical RMS vibrations on wheel and calliper, brake cylinder pressure, vehicle speed

### Behaviour of the Braking System During Line Tests

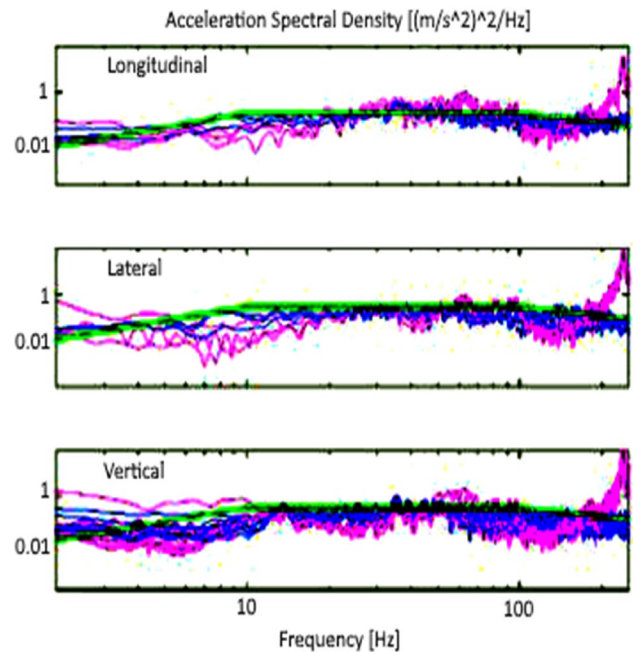
An extensive measurement campaign was performed on the vehicle using accelerometers as shown in Fig. 3. Microphones below the vehicle as well as in the passenger area within the carbody were also installed. Very high N and V levels were confirmed, with unacceptable annoyance inside the vehicle.

Figure 4 shows an example of the test run results (including starting, constant speed and stopping phases) in terms of wheel and calliper longitudinal and vertical acceleration. Wheel accelerations (red lines) are mainly constant during the run, depending only on the vehicle speed. These vibrations are not transferred to the bogie frame (and the brake calliper) due to the filtering effect of the primary suspension.

On the other hand, calliper accelerations (blue lines) result higher than wheel accelerations when braking is applied ( $p > 0$  in the brake cylinder) showing that the abnormal vibrations ( $> 15$  g) in the braking elements were not correlated to wheel vibrations and/or track geometry quality. It was not surprising observing fatigue failures on the callipers under accelerations of this level as design loads are  $\pm 6$  g in vertical direction and  $\pm 2.5$  g in longitudinal direction for components attached to the bogie frame [24].

The accelerations recorded during the measuring campaign were used with a double purpose:

- Validate the design vs. existing standards conducting a frequency analysis according to the EN 61373 standard [25], which defines the requirements for rolling stock equipment subjected to vibrations up to 250 Hz. The



**Fig. 5** Vibration analysis conducted according to EN 61373 [25] on brake calliper. The green line is the spectral density limit, blue lines are the acceleration spectra without braking and purple lines are the acceleration spectra when braking is applied

results of the analysis showed that vibration levels in all directions exceed the limits stated by the standard at around 230 Hz (Fig. 5).

- Performing an operational deflection shape (ODS) analysis [26] integrating twice the acceleration signals with a very low cut-off frequency high-pass filter to prevent data drifting. After the integration process (that acts as a low-pass filter) the only dominant frequency was the one around 220~230 Hz and the resulting displacements let to visualize the two sides of the calliper moving in counterphase (Fig. 6).

### Experimental Frequency Response of the Wheelset

To investigate the frequency response of the wheelset, a simplified frequency response functions (FRF) were measured by hitting vertically and transversally with an instrumented hammer the centre of the axles of a spare wheelset resting on soft rubber blocks placed under the axle boxes [27]. The acceleration was measured during a roving hammer excitation in different positions of the wheelset, allowing to identify the natural modes of the free wheelset.

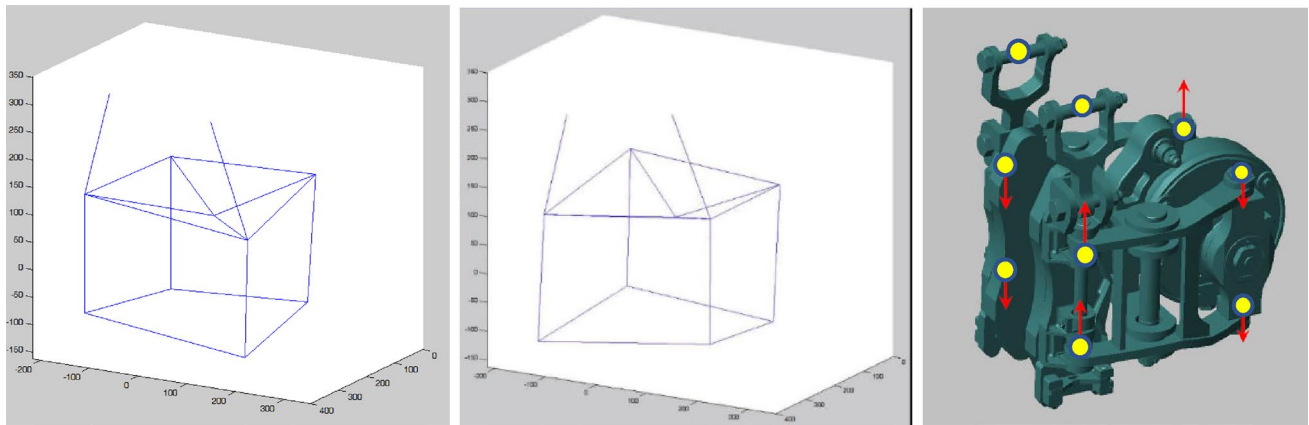
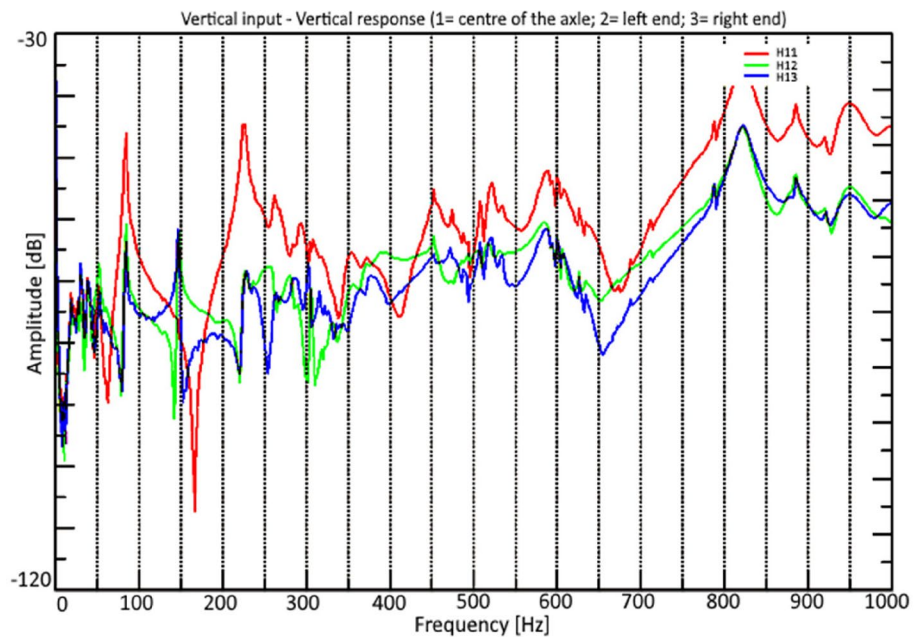


**Fig. 6** Two frames of the animation of the measuring locations on the calliper during braking, plotting the unfiltered full displacement time history that was clearly dominated by the 220~230 Hz movement. The vertical segments are the links connecting the pad hold-

ers to the brake support. Right, a sketch of the full calliper with red arrows reproducing the actual displacements of the evaluated points (yellow dots)

**Fig. 7** Vertical  $H_{11z}$  (red line) and longitudinal point FRFs. The first two peaks are at around 80 Hz and 230 Hz in both FRFs



Measurements were performed with a frequency resolution of 1 Hz in the range 0~1000 Hz. The correlation (coherence) between the input (force) and the output (acceleration) signals was checked by averaging five FRFs per measuring point.

The most relevant result is the point FRFs in vertical direction  $H_{11z}$  shown in Fig. 7 (red line) in which a clear resonance around 230 Hz can be identified.

### Numerical Simulations of the Wheelset

A three-dimensional model of the complete wheelset was developed to perform a FE analysis. Steel properties (Young

modulus  $E=2.1 \times 10^5$  MPa), were used to model the axle, the wheels and the disc hub on which five cast iron disc sectors are bolted. Cubic elements were used to generate a mesh with a minimum element size of 10 mm.

The finite element model was used to estimate numerically the modal properties and the harmonic response up to 1 kHz. The analysis was not intended to exactly replicate the magnitude of the wheelset response and therefore only two combinations of parameters influencing the peaks values were used: a low damping (damping ratio  $\xi=0.001$ ) with adaptive frequency resolution which increases the  $\Delta f$  in proximity of the natural frequencies, and a higher

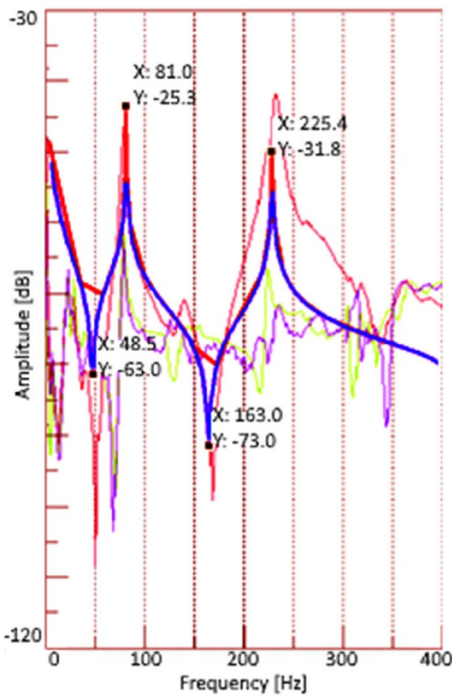


**Fig. 8** Comparison of measured and estimated  $H_{11x}$  point FRFs. Thin red line: measured FRF. Thick red line:  $\xi=0.001$  estimated FRF with variable frequency resolution. Blue thick line,  $\xi=0.01$  estimated FRF with constant frequency resolution

damping (damping ratio  $\xi = 0.01$ ) with fixed frequency resolution equal to  $\Delta f = 1$  Hz.

Damping was applied as constant damping ratio in the whole range of frequencies and the comparison of the two methods with the measured FRF (Fig. 8) shows that both the numerical models are sufficiently tuned to the real behaviour of the wheelset. However, the fixed frequency resolution method was chosen for all the other simulations as it allows a better estimation of anti-resonances.

Further FRFs were then estimated by introducing an inclined triaxial force  $F = 1i + 1j + 1k$  acting at the contact point while the response was evaluated on the surface of the nearby brake disc. A point laying on the horizontal plane on the mid radius of the active surface of the brake disc was selected. The choice of the input value was arbitrary and the real response to wheel–rail contact forces was not searched. The scope of this simulation was instead to check if all the modes can be excited by a generalized force and if the response of the disc was relevant in the whole selected frequency range regardless of the actual contact forces.

The elastic mode shapes up to 400 Hz of the free wheelset obtained by the FEM model are listed and described in Annex I, while the FRF with the indication of the corresponding modes is shown in Fig. 9. Blue line is the

**Fig. 9** Estimated response of one point on the disc active surface on the horizontal plane (mid radius) when excited by a triaxial force at the wheel–rail contact. Orange labels numbering refer to modes listed in Annex I

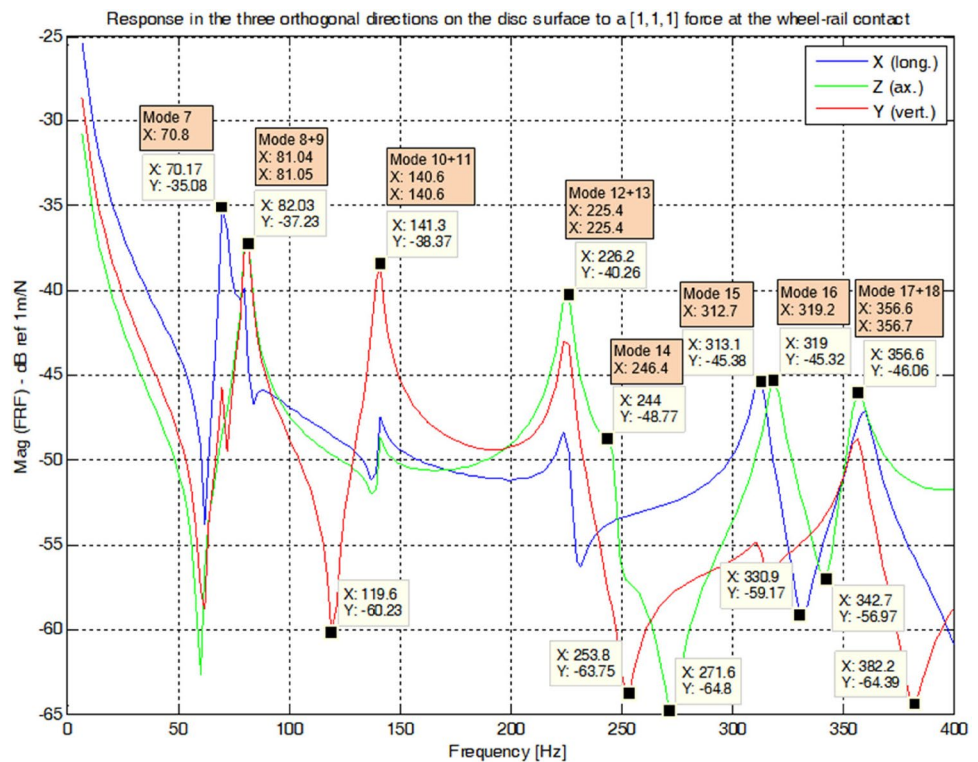
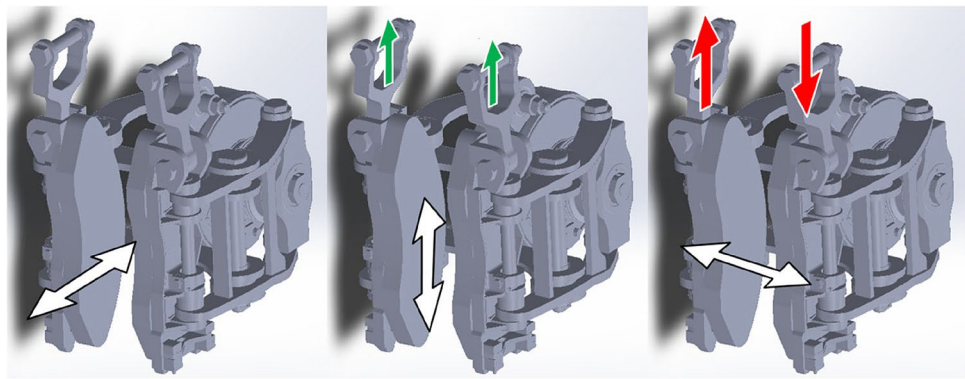




**Fig. 10** Possible mutually orthogonal motions of the disc w.r.t. the brake pads (white arrows). Vertical arrows indicate the change in the instantaneous braking force



longitudinal direction, green line is lateral (axial) direction, and red line represent the vertical direction.

### Identification of the Root Cause

While a brake unit is designed to give the same force to either side of the brake disc, inertial and elastic forces at even low frequencies break this equilibrium and the interaction between the disc and the brake unit can be affected by three linear motions, as shown in Fig. 10:

- If the disc moves longitudinally (in plane), there is no change in the braking forces.
- If the disc moves vertically (in plane), the change of the braking forces on both sides of the calliper is identical (in phase) and of limited amplitude (therefore unable to trigger stick–slip phenomena);
- If the disc moves laterally (out-of-plane) the normal forces applied by the pads change considerably, resulting in similar change on the vertical forces. These forces act with opposite phase, i.e. shearing forces.

The kind of motion resulting from the ODS analysis is compatible with this out-of-plane movement. It was therefore concluded that the generation of vibrations could be originated by the shearing forces which are generated by the out-of-plane motion of the brake disc due to the dynamic response of the wheelset to wheel–rail contact forces. In this way, all the mode shapes not involving a lateral motion of the brake disc are excluded from being responsible for vibration.

According to the previously described FEM model, modal shapes with out-of-plane movements of the brake disc surface are modes 8 and 9 (~81 Hz, large effect), modes 10 and 11 (~141 Hz, small effect), modes 12 and 13 (~225 Hz, large effect), mode 14 (~246 Hz, small effect), mode 16 (~319 Hz, large effect), modes 17 and 18 (~357 Hz, large effect). Modes 7 (~71 Hz) and 15 (~313 Hz) should have instead no effect at all.

As modes 12 and 13 are the closest to the frequency found during the measuring campaign and they show relevant out-of-plane movements, the root cause was identified as the coincidence of the third natural bending frequency of the wheelset and the “twisting” mode of the braking systems that are “short-circuited” by the pads during braking.

### Response of the Bogie Frame to Shearing Forces

The combined bogie frame + brake support + brake unit response to the alternate shearing forces described above was numerically investigated. While the number of natural frequencies of a full bogie frame is large, it is reasonable to suppose that the analysis can be limited to the submodel made of the braking bar, the welded bracket and the brake support, as shown in Fig. 11.

The finite element model was tuned manually changing the masses of the calliper to obtain modes that match with the tests. This led to 18 kg each for the two front masses (brake pads and pad holders) and to 40 kg for the rear mass (brake cylinder). These values are in complete agreement with real masses of the mechanical components. To improve

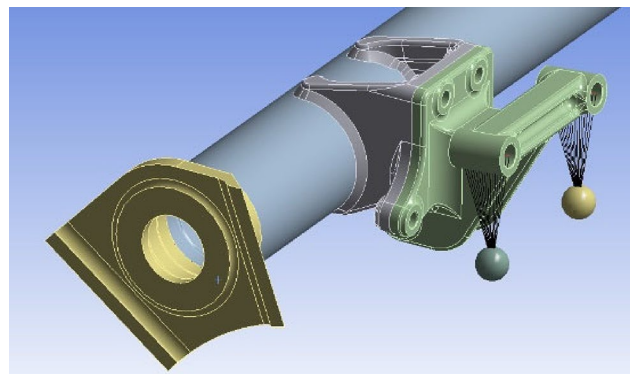
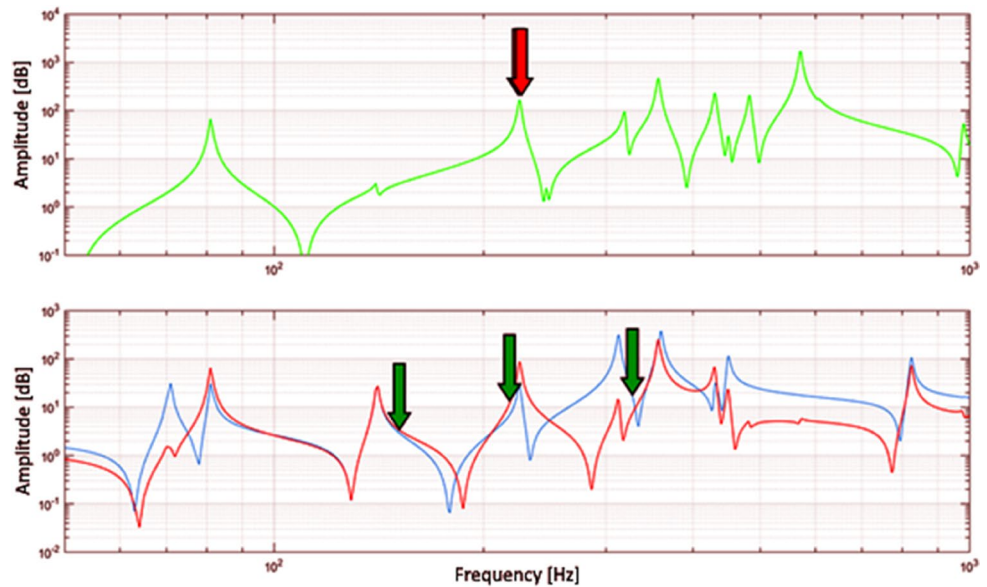


**Fig. 11** Submodel of the brake support, the braking bar and the welded bracket

**Fig. 12** Comparison of axial (above) and radial (below) response of the wheelset with the natural modes of the bogie submodel shown in Annex II indicated separately for twist (red arrows) and pitch modes (green arrows)



the dynamic behaviour of the model, the two front masses were connected remotely by means of cylindrical frictionless hinges to the brake support inclined by  $5^\circ$  as the real component.

The first modes of the tuned bogie submodel are described in Annex II. They were classified according to the main motion of the calliper supports as “pitch modes” (“eyes” move vertically in phase) and “twist modes” (“eyes” move vertically in counterphase).

The axial response of the wheelset (Fig. 12, above) may generate “twist” forces coupled with modes 3 and 4 of the bogie submodel (red arrows), while the response in the radial/longitudinal direction (Fig. 12, below) may generate “pitch” forces coupled with modes 1, 2 and 5 of the bogie submodel (green arrows).

For reasons related to the possible modifications to be applied, as shown in the next chapter, it is important to highlight a dangerous area in the range 300~600 Hz due to the presence of several modes in the axial response of the wheelset (Fig. 12, above).

As pitch modes of the brake support are deemed to be of minor importance for the reasons described in chapter 3, the interest was then focused on the very close twist modes 3 and 4 (counterphase at  $\sim 226$  Hz and in phase at  $\sim 228$  Hz) of the brake supports (Fig. 13).

### Proposed Modifications to the Brake Support

As no changes were possible to the bogie frame, to the wheelset and the to brake calliper as these safety-related components were approved for service and a re-certification of the vehicle had to be absolutely avoided, the only possibility was to investigate the effect of several modifications to the existing brake supports either by changing the ribs stiffness or by designing a totally new brake support, clearly keeping unchanged the interface to both the bogie and the calliper.

To break the coincidence of the natural frequency of the bogie frame submodel with the natural frequency of

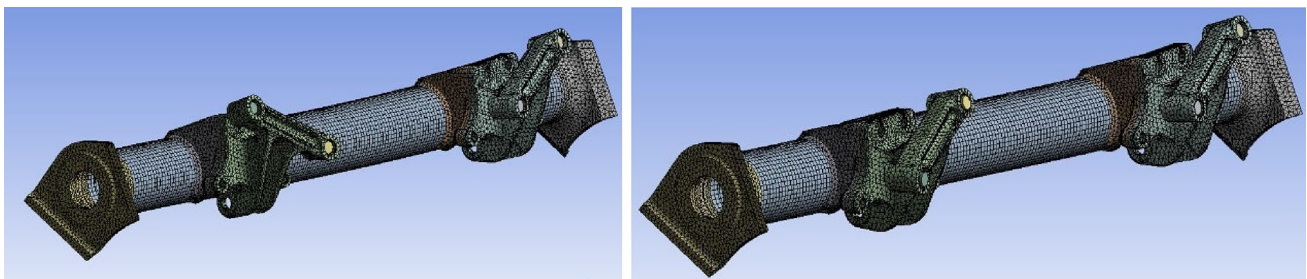


**Fig. 13** Counterphase (left, 226 Hz) and in-phase (right, 228 Hz) brake support natural modes of the bogie submodel



the wheelset that excited shearing forces, the formula  $f = (k/m)^{1/2}/2\pi$  that provides the natural frequency  $f$  of single degree of freedom systems with stiffness  $k$  and mass  $m$ , had to be considered. Structural modifications of the brake support were grouped in those decreasing the natural frequency (either by increasing the masses (A) or by reducing the stiffness of brake support (B)) and in those increasing the natural frequency (either by increasing the stiffness (C) or by decreasing the mass of the brake support (D)) of the bogie frame submodel.

While modification D proved not possible for mechanical strength reasons, solutions A, B and C were investigated as the final selection had to be done not only on the basis of the dynamic behavior, but also evaluating manufacturing and maintenance parameters.

Solution A consisted in the addition of steel blocks (6.4 kg each) clamped to the existing brake support was simulated, taking into account the fact that the brake support is a casting and that therefore the solution should be self-adjusting (Fig. 14).

This solution requires no machining of the support, steel blocks can be applied without any further operation, the design is compatible with adjacent parts, the installation is fast, there is no need to lift the car body up for

installation and the train is immediately available to go back to service.

The effect of these masses is to reduce the twisting frequency from around 227–189 Hz, looking very promising. The only concern was about inertial forces; however, considering the limits stated in [24], these inertia forces are equal to 0.4 kN with 6 g acceleration (fatigue loads) and 1.3 kN with 20 g acceleration (exceptional loads). These values are negligible when compared to the maximum braking forces (> 20 kN) under which the support is designed.

Solution B consisted in softening the brake supports by removing small portions of the vertical ribs (Fig. 15). This solution requires very simple machining (slot milling, tool  $d = 20$  mm) without hot operations (welding, laser cutting, etc.).

The effect of these solution is to reduce the twisting frequency from around 227–191 Hz, looking very promising. The only concern was about strength of the component after milling. Under the maximum braking forces the maximum equivalent stress according to the Von Mises criterion is lower than 170 MPa, below the fatigue limit of the material.

Solution C consisted in stiffening the brake support. This can be done in many ways. By using an extreme solution, in which the original support was replaced by a thick

**Fig. 14** CAD drawing of the addition of a 6.4 kg mass at each end of the brake support upper element (left). Simplified implementation on the FEM dynamic model (right)

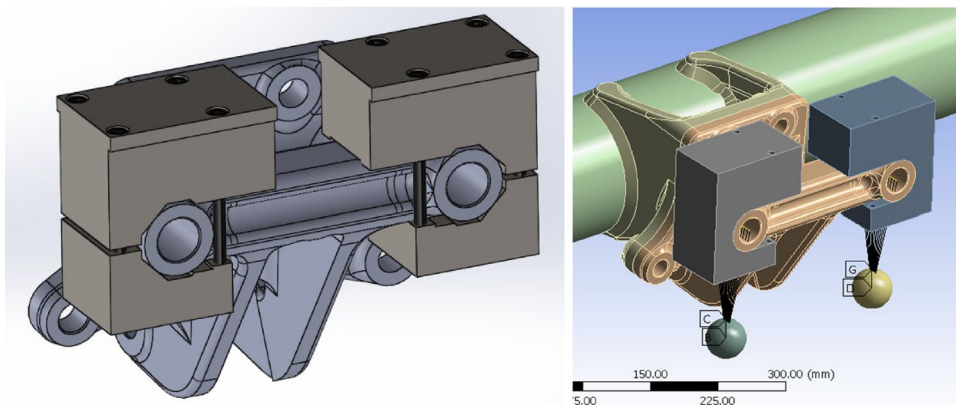


**Fig. 15** CAD drawing of the softer brake support (left). Simplified implementation on the FEM dynamic model (right)

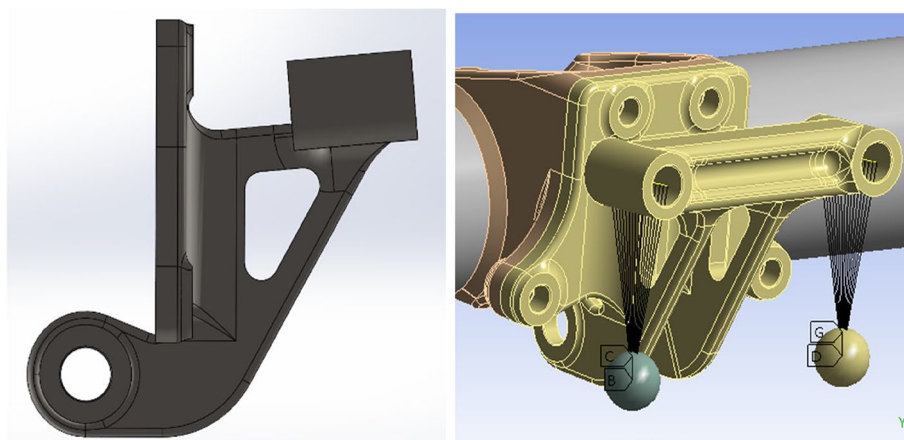


**Fig. 16** FE implementation of an extremely stiff support (left). First twisting mode, at 562 Hz (right)

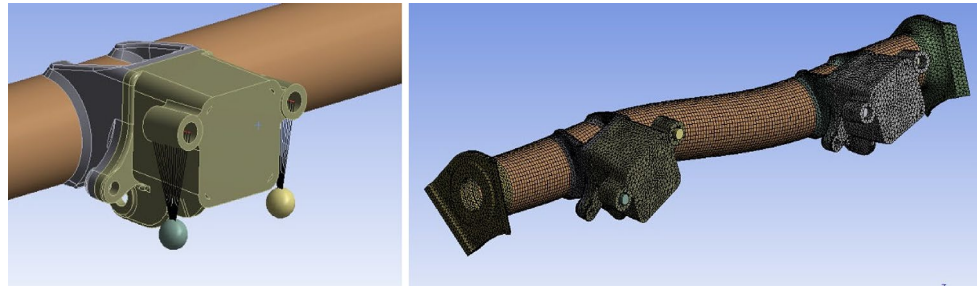
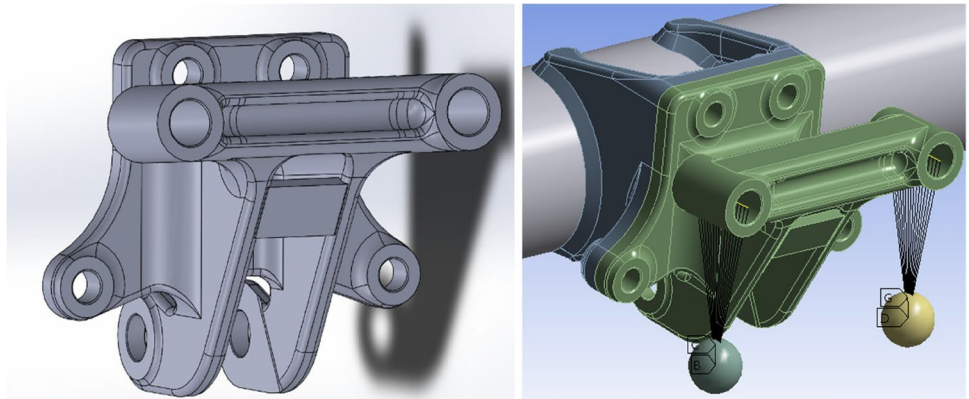


**Fig. 17** CAD drawing of a small stiffening rib applied to the existing brake support (left) and FE model (right)



160 × 160 × 12.5 mm square steel pipe to which a rear plate and the “eyes” are welded (Fig. 16), the analysis of the isolated support (fixed at the rear) showed a twist frequency of around 775 Hz, i.e. outside the dangerous 300 ÷ 600 Hz range described above. Unfortunately, when applied to the bogie frame the same mode appeared at 562 Hz, i.e. coincident in practice with a high lateral response of the brake disc. This is mainly due to the flexibility of the bracket welded on the braking bar. It was concluded that it was necessary to modify the bogie frame to go beyond the dangerous 300 ÷ 600 Hz range.

Once the idea of a totally new support was abandoned, several stiffeners were applied to the existing brake support. The only possibility was then to try to “fall” in the anti-resonance region existing at around 250 Hz and the best solution found is shown in Fig. 17, in which the adoption of a simple 40-mm-long horizontal transversal rib connecting the vertical ribs is shown.

This solution requires a very simple preparation and simple welding operations. The effect of these solution is to increase the twisting frequency from around 227–244 Hz.

A comparison of the effect of the structural modifications above on the bogie frame submodel in nominal conditions (i.e. with new pads) is shown in Fig. 18.

After a long and thorough comparison, solution C was selected as the best combination of simplicity and potential efficacy.

**Summary of main twist natural frequencies**

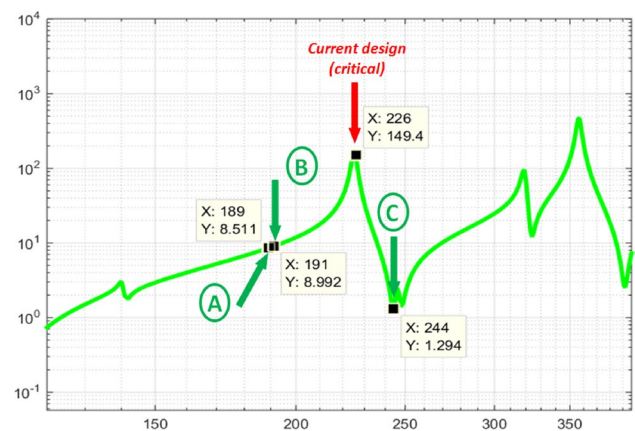
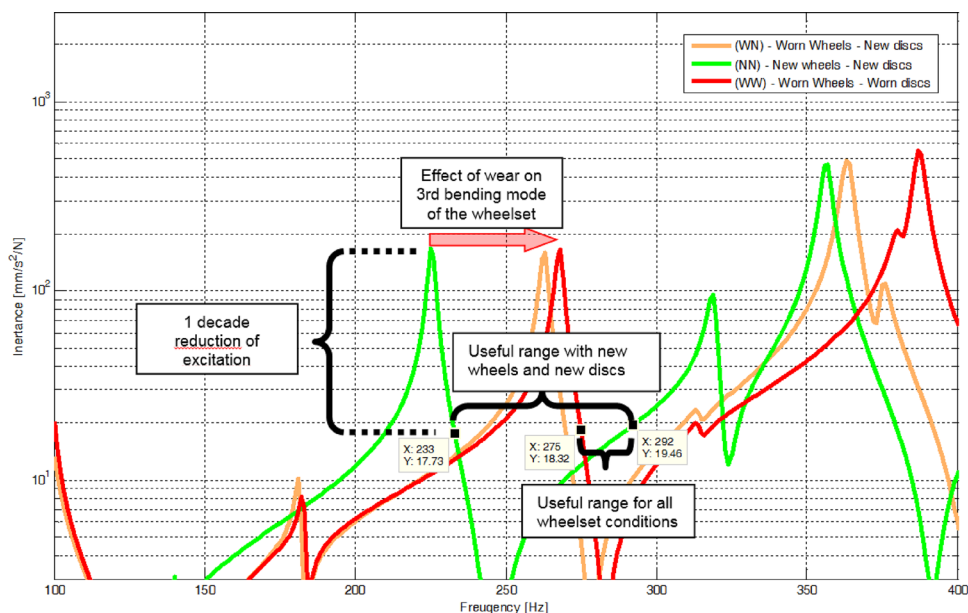


**Fig. 18** Effect on the twisting frequency of the different structural modifications proposed for the brake calliper support (green arrows) compared to the current twisting frequency (red arrow)

## Sensitivity and Robustness Analyses

The target of the modification was set to reduce vibrations by one order of magnitude. As the damping of the bogie frame submodel was unaffected by stiffening, this can be achieved only by acting on the response of the braking system to wheelset vibrations that depend on the level of wear of its components. Specific simulations were performed to

**Fig. 19** Change of the natural frequencies of the wheelset in wheels and discs new and worn conditions



analyse the system in all possible combinations of wear of the different components (wheel, brake discs, brake pads), making the solution highly robust under all service conditions. Results are shown in Fig. 19.

The amplitude of the excitation coming from the wheelset is reduced by a factor 10 in the 233 ÷ 292 Hz useful range. The proposed 40-mm-long stiffener (solution C) is therefore an effective solution with the wheelset in new conditions as its natural frequency lies in this range (244 Hz),

The combined effect of wheel wear (– 80 kg each from new to fully worn) and brake discs wear (– 20 kg each from new to fully worn) leads to a gradual shift of the wheelset modes towards higher frequencies. This implies that the useful range for bogie frame submodel reduces to the 275 ÷ 292 Hz range, making solution C with 40-mm stiffener unsuitable.

This sensitivity analysis forced to look for a different solution able to cover all worn conditions of the wheelset. To be robust, a solution must be effective with all the “natural” modifications of the mechanical system that, in the long term, is not time invariant.

Further to the effect of wheel and brake discs wear on the wheelset natural frequencies, also the effect of worn brake pads (– 2 kg each) on the bogie submodel was investigated.

A set of simulations was made to combine all possible wear conditions. The resulting natural frequencies and the influence of the length of the stiffener are summarized in Table 1 and Fig. 20. It proved impossible to completely fulfil the 275–292 Hz range by a stiffening of any length as the shift between the in-phase and the counterphase motion frequency of the two brake supports only depends on the braking bar stiffness, a parameter that cannot be changed. It was eventually decided to select a 80-mm-long stiffener that provides a reduction of approximately 0.13 times the nominal situation.

### Testing and Validation of the Modified Calliper Support

Both an original support and a modified support with an 80-mm-long stiffener were tested to validate the activity (Fig. 21). As some eigenmodes are local and a total

**Table 1** List of natural frequencies of twisting modes of the bogie frame submodel as a function of the length of the stiffener and of the wear of brake pads (green=OK, red=not OK, yellow = still acceptable)

| Length of the stiffener | 18 kg per side (new brake pads) |                      | 16 kg per side (worn brake pads) |                      |
|-------------------------|---------------------------------|----------------------|----------------------------------|----------------------|
|                         | Counterphase motion [Hz]        | In-phase motion [Hz] | Counterphase motion [Hz]         | In-phase motion [Hz] |
| 0                       | 226 Hz                          | 228 Hz               | 238 Hz                           | 241 Hz               |
| 40 mm                   | 244 Hz                          | 247 Hz               | 256 Hz                           | 261 Hz               |
| 60 mm                   | 259 Hz                          | 265 Hz               | 271 Hz                           | 280 Hz               |
| 80 mm                   | 272 Hz                          | 285 Hz               | 285 Hz                           | 300 Hz               |
| 90 mm                   | 278 Hz                          | 292 Hz               | 289 Hz                           | 308 Hz               |
| 120 mm                  | 285 Hz                          | 305 Hz               | 296 Hz                           | 322 Hz               |



**Fig. 20** Plot of the data shown in Table 1 (natural frequencies of the bogie submodel as a function of brake pad wear and stiffener length). The shaded area is the range  $275 \div 292$  Hz in which the wheelset response is  $< 0.1$  times the amplitude of the resonance for any wheelset wear condition

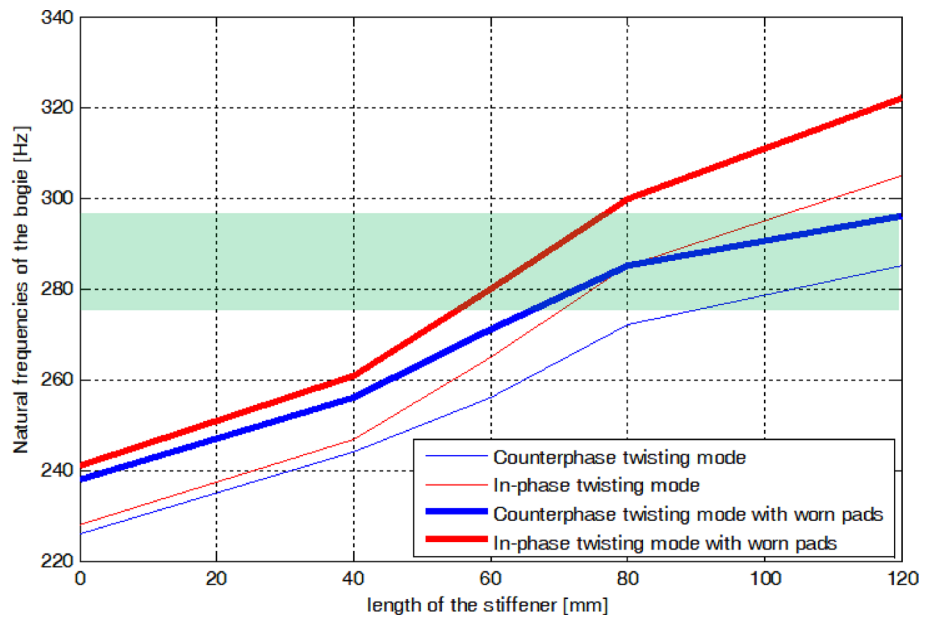


**Fig. 21** Left: a modified support with an 80-mm welded stiffener. Right: measurement of the point FRF on both original and modified support



correspondence of the numerical model with the experimental tests is impossible, it was decided to focus only on the global modes (so-called target modes) and to update the model with minor adjustment in the geometry of the component. In both supports, the bushings (missing in the previous analyses) were introduced. The comparison between FEM and the result of the tests is shown in Annex III, showing that the models used in the original calculations were satisfactory. A further re-calculation of the braking bar led to negligible changes in the natural frequencies.

## Testing, Application and Final Considerations

To solve the issue of groan noise appearing in the trailer bogie of an upgraded metro vehicle, the authors investigated first the natural behaviour of the mechanical and friction system, reaching the conclusion that the root cause was due to the coincidence of the natural frequencies of

the wheelset and of the part of the bogie frame including the braking system.

To break the tie between the two subsystems, a shift in the natural frequencies to decouple them was searched for. Through an extensive modelling and tuning phase based on experimental data, a solution was found by a relatively simple structural modification of the calliper support. A sensitivity analysis of system changes due to the wear of the components involved in the phenomenon (wheel wear, disc wear, brake pads wear) was needed to make the solution robust throughout the entire life of the vehicle.

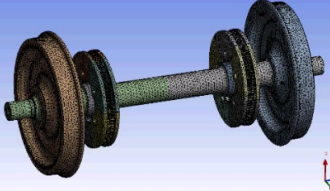
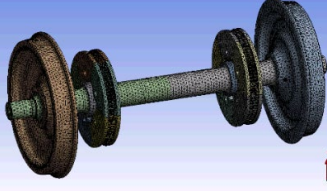
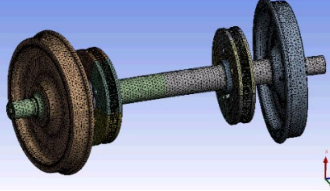
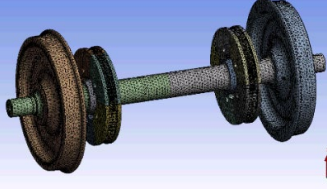
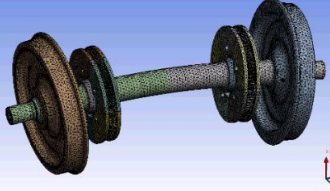
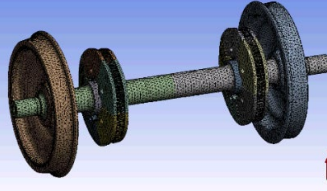
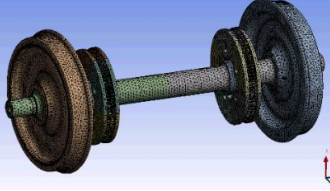
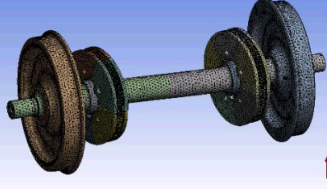
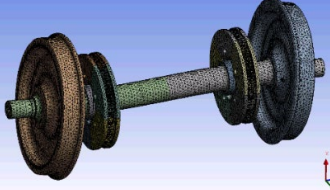
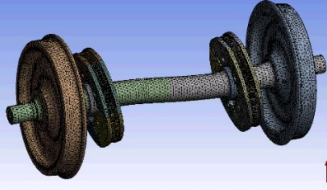
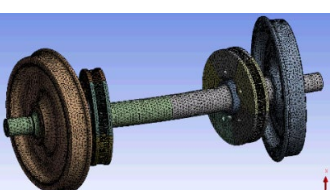
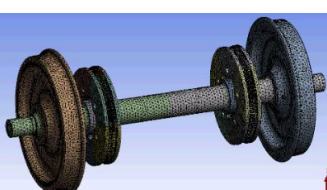
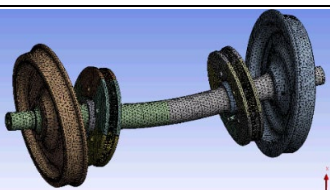
All the vehicles in the fleet were gradually retrofitted with the modified solution without showing the problem anymore. No noise and/or vibrations were then perceived during the service, making any further measuring unnecessary.

The modification had a minimum impact on operations, as the bogie frame, the wheelset and the braking unit were not affected by the brake support replacement. As there was no practical effect on the mass, a re-homologation of the vehicle was not needed.

It can be concluded that the application of a very robust and low-cost modification solved the issue completely. Also other side effects, such as abnormal brake pads wear, disappeared.

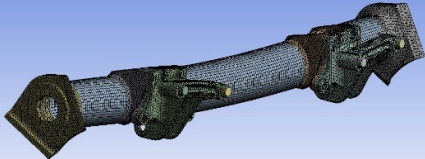
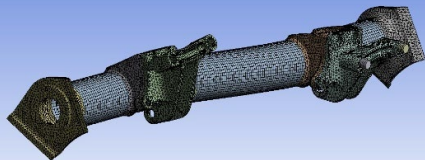
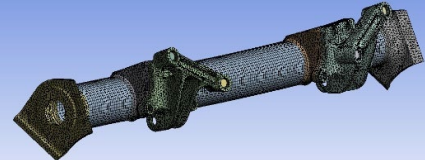
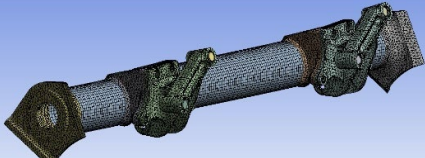
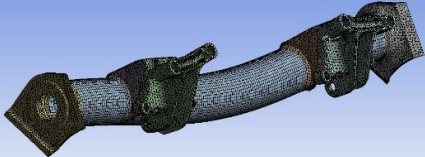
### Annex I

List of numerical elastic mode shapes and natural frequencies of the free wheelset in the frequency range of interest (\* = lateral motion of the discs on a horizontal plane passing through the axle). Rigid body modes (1 ~ 6) are omitted.

| Mode description   | Mode shape  | Mode description  | Mode shape  |
|--|---|---|---|
| <b>Mode 7 (71 Hz)</b><br>1 <sup>st</sup> torsional mode<br>(wheels and discs on each side in phase)<br><i>In-plane motion of the discs*</i>                |    | <b>Mode 14 (246 Hz)</b><br>Axial mode of the wheels<br><i>Small out-of-plane motion of the discs*</i>   |    |
| <b>Mode 8 (81 Hz)</b><br>1 <sup>st</sup> horizontal bending mode of the axle<br><i>Out-of-plane motion of the discs*</i>                                   |    | <b>Mode 15 (313 Hz)</b><br>2 <sup>nd</sup> torsional mode (wheel and discs on each side in counterphase)<br><i>In-plane motion of the discs*</i>        |    |
| <b>Mode 9 (81 Hz)</b><br>1 <sup>st</sup> vertical bending mode of the axle<br><i>No motion of the discs*</i>   |   | <b>Mode 16 (319 Hz)</b><br>Axial mode wheels and discs in counterphase<br><i>Out-of-plane motion of the discs*</i>                                      |   |
| <b>Mode 10 (141 Hz)</b><br>2 <sup>nd</sup> horizontal bending mode<br><i>Small out-of-plane motion of the discs*</i>                                       |  | <b>Mode 17 (357 Hz)</b><br>2 <sup>nd</sup> horizontal bending mode of the axle with discs large motion<br><i>Out-of-plane motion of the discs*</i>      |  |
| <b>Mode 11 (141 Hz)</b><br>2 <sup>nd</sup> vertical bending mode<br><i>Small out-of-plane motion of the discs*</i>   |  | <b>Mode 18 (357 Hz)</b><br>2 <sup>nd</sup> vertical bending mode of the axle with discs large motion<br><i>Small out-of-plane motion of the discs*</i>  |  |
| <b>Mode 12 (225 Hz)</b><br>1 <sup>st</sup> horizontal bending mode of the axle with wheels in counterphase<br><i>Out-of-plane motion of the discs*</i>     |  | <b>Mode 19 (360 Hz)</b><br>3 <sup>rd</sup> torsional mode, discs in counterphase, small movements of the wheels<br><i>In-plane motion of the discs*</i> |  |
| <b>Mode 13 (225 Hz)</b><br>1 <sup>st</sup> vertical bending mode of the axle with wheels in counterphase<br><i>Small out-of-plane motion of the discs*</i> |  |   |   |

## Annex II

List of mode shapes and natural frequency up to 500 Hz of the bogies frame submodel. Modes are identified based on the dominant displacement component as “twist” (“eyes” in counterphase) and “pitch” (“eyes” in phase).

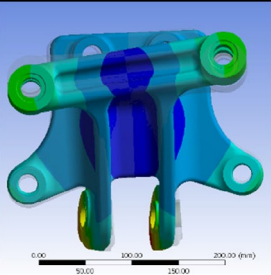
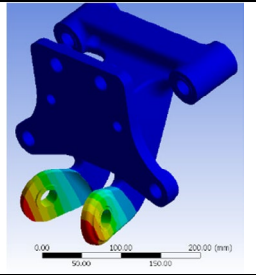
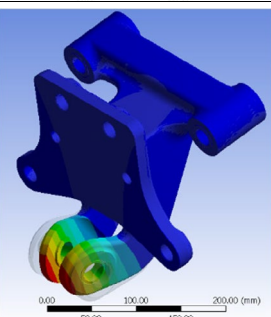
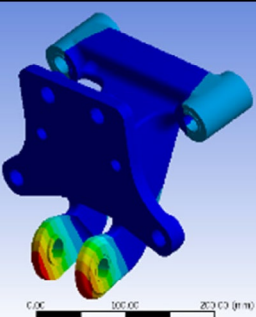
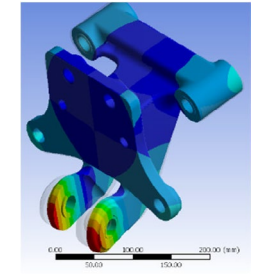
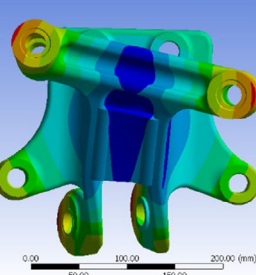
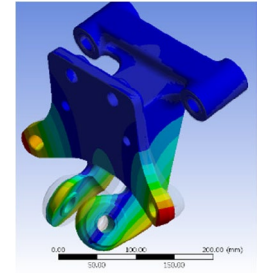
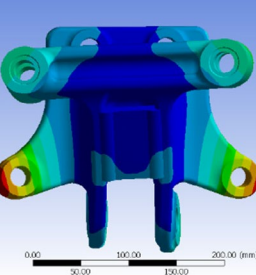
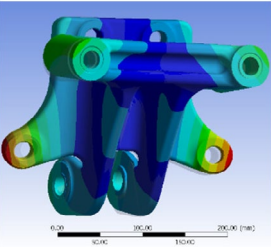
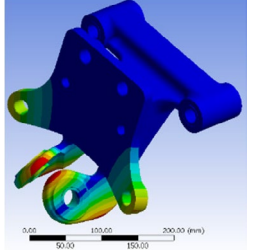
| Mode # | Freq. [Hz] | Mode shape  | Description   |
|--------|------------|---|---|
| 1      | 156        |    | 1 <sup>st</sup> “pitch” mode (supports in phase)        |
| 2      | 211        |    | 2 <sup>nd</sup> “pitch” mode (supports in counterphase) |
| 3      | 226        |    | 1 <sup>st</sup> “twist” mode (supports in counterphase) |
| 4      | 228        |  | 2 <sup>nd</sup> “twist” mode (supports in phase)        |
| 5      | 324        |  | 3 <sup>rd</sup> “pitch” mode (supports in phase)        |



**Annex III**

Tuning of the models of original and modified support (80-mm-long stiffener). Green cells identify the modes that

were selected to get the lowest error between experimental and numerical natural frequencies.

| Mode | Original support  |  | Modified (stiffened) support   |  |
|------|---|--|--|--|
|      | Mode shape  | Frequency  | Mode shape   | Frequency  |
| 1    |    | Original= 894 Hz<br>Tuned= 863 Hz<br>Experimental= 864 Hz<br>Error= -0.1%    |    | Original= 935 Hz<br>Tuned= 902 Hz<br>Experimental= 934 Hz<br>Error= -3.5%    |
| 2    |   | Original= 913 Hz<br>Tuned= 874 Hz<br>Experimental= 881 Hz<br>Error= -0.8%    |   | Original= 978 Hz<br>Tuned= 951 Hz<br>Experimental= 977 Hz<br>Error= -2.7%    |
| 3    |  | Original= 1049 Hz<br>Tuned= 1017 Hz<br>Experimental= 1022 Hz<br>Error= -0.5% |  | Original= 1479 Hz<br>Tuned= 1485 Hz<br>Experimental= 1492 Hz<br>Error= -0.5% |
| 4    |  | Original= 1775 Hz<br>Tuned= 1774 Hz<br>Experimental= 1834 Hz<br>Error= -5.1% |  | Original= 1956 Hz<br>Tuned= 1945 Hz<br>Experimental= 1939 Hz<br>Error= +0.3% |
| 5    |  | Original= 1951 Hz<br>Tuned= 1907 Hz<br>Experimental= 1963 Hz<br>Error= -2.9% |  | Original= 1969 Hz<br>Tuned= 1983 Hz<br>Experimental= 1995 Hz<br>Error= -0.6% |

**Funding** Open access funding provided by Università degli Studi di Firenze within the CRUI-CARE Agreement.

## Declarations

**Conflict of Interest** The authors have no conflict of interest to declare.

**Open Access** This article is licensed under a Creative Commons Attribution 4.0 International License, which permits use, sharing, adaptation, distribution and reproduction in any medium or format, as long as you give appropriate credit to the original author(s) and the source, provide a link to the Creative Commons licence, and indicate if changes were made. The images or other third party material in this article are included in the article's Creative Commons licence, unless indicated otherwise in a credit line to the material. If material is not included in the article's Creative Commons licence and your intended use is not permitted by statutory regulation or exceeds the permitted use, you will need to obtain permission directly from the copyright holder. To view a copy of this licence, visit <http://creativecommons.org/licenses/by/4.0/>.

## References

- Thompson D, Latorre Iglesias E, Liu X, Zhu J, Hu Z (2015) Recent developments in the prediction and control of aerodynamic noise from high-speed trains. *Int J Rail Transp* 3(3):119–150. <https://doi.org/10.1080/23248378.2015.1052996>
- Liu X, Zhang J, Thompson D, Iglesias EL, Squicciarini G, Hu Z et al (2021) Aerodynamic noise of high-speed train pantographs: comparisons between field measurements and an updated component-based prediction model. *Appl Acoust*. <https://doi.org/10.1016/j.apacoust.2020.107791>
- Shimokura R, Soeta Y (2011) Characteristics of train noise in above-ground and underground stations with side and island platforms. *J Sound Vib* 330(8):1621–1633
- Lorang X, Foy-Margiocchi F, Nguyen QS, Gautier PE (2006) TGV disc brake squeal. *J Sound Vib* 293(3–5):735–746. <https://doi.org/10.1016/j.jsv.2005.12.006>
- Chiello O, Sinou JJ, Vincent N, Vermot des Roches G, Cochetoux F, Bellaj S, et al. (2013) Squeal noise generated by railway disc brakes: Experiments and stability computations on large industrial models. 21st International Congress on Acoustics, 165th Meeting of the Acoustical Society of America, 52nd Meeting of the Canadian Acoustical Association, Jun 2012, Montréal, Canada
- Eriksson M, Bergman F, Jacobson S (2002) On the nature of tribological contact in automotive brakes. *Wear* 252(1):26–36. [https://doi.org/10.1016/S0043-1648\(01\)00849-3](https://doi.org/10.1016/S0043-1648(01)00849-3)
- Cascetta F, Caputo F, De Luca A (2018) Squeal frequency of a railway disc brake evaluation by FE analyses. *Adv Acoust Vib*. <https://doi.org/10.1155/2018/4692570>
- Kim K, Yoo N, Lee E (2022) Vibrational instability analysis for railway brake system equipped with flexible pad structure. *IntJ Automot Technol* 23(4):1117–1125. <https://doi.org/10.1007/s12239-022-0098-7>
- Wu Y (2020) Mechanism analysis of a low-frequency disc brake squeal based on an energy feed-in method for a dual coupling subsystem. *Shock Vib*. <https://doi.org/10.1155/2020/8887529>
- Tison T, Heussaff A, Massa F, Turpin I, Nunes RF (2014) Improvement in the predictivity of squeal simulations: uncertainty and robustness. *J Sound Vib* 333:3394–3412. <https://doi.org/10.1016/j.jsv.2014.03.011>
- Do HQ, Massa F, Tison T, Lallemand B (2017) A global strategy for the stability analysis of friction induced vibration problem with parameter variations. *Mech Syst Signal Process* 84:346–364. <https://doi.org/10.1016/j.ymsp.2016.07.029>
- Rao M, Frank J, Kohli M (2014) Diagnosis and Elimination of Disc Brake Groan in a Utility Vehicle. SAE Tech Paper. <https://doi.org/10.4271/2014-01-0043>
- Doundkar V, Iqbal S (2021) Brake groan noise investigation and optimization strategies for passenger vehicles. SAE Tech Paper. <https://doi.org/10.4271/2021-26-0301>
- Neis PD, Ferreira NF, Poletto JC, Matozo LT, Masotti D (2016) Quantification of brake creep groan in vehicle tests and its relation with stick–slip obtained in laboratory tests. *J Sound Vib* 369:63–76. <https://doi.org/10.1016/j.jsv.2016.01.036>
- Zhao X, Gräbner N, Von Wagner U (2018) Theoretical and experimental investigations of the bifurcation behavior of creep groan of automotive disk brakes. *J Theor Appl Mech* 56:351–364. <https://doi.org/10.15632/jtam-pl.56.2.351>
- Megna G, Bracciali A (2023) Solving groan noise problems in a metro braking system. In: Dimitrovová Z, Biswas P, Gonçalves R, Silva T (eds) Recent trends in wave mechanics and vibrations. WMVC 2022. Mechanisms and machine science, vol 125. Springer, Cham. [https://doi.org/10.1007/978-3-031-15758-5\\_65](https://doi.org/10.1007/978-3-031-15758-5_65)
- Brennan MJ, Shin K (2007) Brake noise prediction and control. In: Crocker MJ (ed) Handbook of noise and vibration control. John Wiley and Sons, Hoboken, pp 1133–1137
- Ghazaly N, Ahmed I, El- Sharkawy M (2014) A review of automotive brake squeal mechanisms. *J Mech Des Vib* 1(1):5–9. <https://doi.org/10.12691/jmdv-1-1-2>
- Bettella M, Harrison MF, Sharp RS (2002) Investigation of automotive creep groan noise with a distributed-source excitation technique. *J Sound Vib* 255(3):531–547. <https://doi.org/10.1006/jsvi.2001.4178>
- Brecht J, Hoffrichter W, Dohle A (1997) Mechanisms of brake creep groan. SAE Tech Paper. <https://doi.org/10.4271/973026>
- Dunlap K, Riehle M, Longhouse R (1999) An investigative overview of automotive disc brake noise. SAE Tech Paper. <https://doi.org/10.4271/1999-01-0142>
- Vadari V, Jackson M (1999) An experimental investigation of disc brake creep-groan in vehicles and brake dynamometer correlation. SAE Tech Paper. <https://doi.org/10.4271/1999-01-3408>
- Donley M, Riesland D (2003) Brake groan simulation for a McPherson strut type suspension. SAE Tech Paper. <https://doi.org/10.4271/2003-01-1627>
- EN 13749:2021, Railway applications—Wheelsets and bogies—Method of specifying the structural requirements of bogie frames
- EN 61373:2010, Railway applications—Rolling stock equipment—Shock and vibration tests, CENELEC, September 2010
- Kromulski J, Hojan E (1996) An application of two experimental modal analysis methods for the determination of operational deflection shapes. *J Sound Vib* 196(4):429–438. <https://doi.org/10.1006/jsvi.1996.0493>
- Bracciali A, Rissone P (1994) Analisi Modale Sperimentale di una Sala Portante del Convoglio ETR500. *Ingegneria Ferroviaria* 7(8):394–407

**Publisher's Note** Springer Nature remains neutral with regard to jurisdictional claims in published maps and institutional affiliations.